DOI: 10.31276/VJSTE.64(3).29-37

Interaction between a complex fluid flow and a rotating cylinder

Cuong Mai Bui[1], Thinh Xuan Ho[2*]

[1]*University of Technology and Education, The University of Danang*
[2]*Department of Computational Engineering, Vietnamese - German University*

Received 27 January 2021; accepted 23 April 2021

Abstract:

The flow of a thixotropic Bingham material past a rotating cylinder is studied under a wide range of Reynolds and Bingham numbers, thixotropic parameters, and rotational speeds. A microstructure transition of the material involving breakdown and recovery processes is modeled using a kinetic equation, and the Bingham-Papanastasiou model is employed to represent shear stress-strain rate relations. Results show that the material's structural state at equilibrium depends greatly on the rotational speed and the thixotropic parameters. A layer around the cylinder resembling a Newtonian fluid is observed, in which the microstructure is almost completely broken, the yield stress is negligibly small, and the apparent viscosity approximates that of the Newtonian fluid. The thickness of this Newtonian-like layer varies with the rotational speed and the Reynolds number, but more significantly with the former than with the latter. In addition, the lift and moment coefficients increase with the rotational speed. These values are found to be close to those of the Newtonian fluid as well as of an equivalent non-thixotropic Bingham fluid. Many other aspects of the flow such as the flow pattern, the unyielded zones, and strain rate distribution are presented and discussed.

Keywords: **Bingham, computational fluid dynamics (CFD), non-Newtonian fluid, thixotropy, yield stress.**

Classification number: **2.3**

Introduction

Non-Newtonian liquids such as sediment [1-4], fresh concrete, and cement [5-7] have rheologically complex characteristics, which can include viscoplasticity, typically of a Bingham type, and thixotropy. Bingham materials flow when an applied shear stress (τ) is greater than a threshold value (τ_0 i.e., yield stress). Otherwise, they behave like a solid. Thixotropy is a characteristic associated with the materials' microstructure that can be broken down and/or built up under shearing conditions. The breakdown process increases their flowability, while the recovery process does the opposite. Good reviews about thixotropy can be found in, e.g., H.A. Barnes (1997) [8], J. Mewis and N. Wagner (2009) [9], and most recently R.G. Larson and Y. Wei (2019) [10]. In a flow field of these materials, solid-like zones where $\tau \leq \tau_0$ can be formed known as unyielded zones; beyond these zones where $\tau > \tau_0$ the materials are yielded and hence behave like liquids.

Thixotropic Bingham liquids are encountered in numerous applications in which interaction between complex liquids and a moving object can be presented. For Newtonian fluids, the fluid-solid interaction is a classical problem in fluid mechanics and has extensively been studied [11-13]. However, only a limited number of works have been found for Non-Newtonian fluids. While a majority of these works dealt with stationary cylinders, only a few examined rotating cylinders.

With a stationary cylinder, D.L. Tokpavi, et al. (2008) [14] investigated the creeping flow of viscoplastic fluid. Size and shape of unyielded zones were found to depend on the Oldroyd number (Od) at low values and asymptote those at $Od=2\times10^5$. S. Mossaz, et al. (2010, 2012) [15-17] explored both numerically and experimentally a yield-stress fluid flow over a stationary cylinder. The flow was laminar with and without a recirculation wake. Aspects such as size of the recirculation wake and unyielded zones were investigated. Recently, Z. Ouattara, et al. (2018) [18] performed a rigorous study of a cylinder translating near a wall in a still Herschel-Bulkley liquid. The flow was at a Reynolds number of Re~0 and both numerical and experimental approaches were employed. Effects of Od and cylinder-wall gap on drag force were reported.

Regarding the flow over a rotating cylinder, several works have been performed, for example, with a shear-thinning viscoelastic fluid [19] and shear-thinning power-

*Corresponding author: Email: thinh.hx@vgu.edu.vn

law fluid [20] at Re≤40. Results of flow pattern as well as drag and lift forces were reported to depend on Re, the cylinder's rotational speed, and the shear-thinning behaviour. In addition, P. Thakur, et al. (2016) [21] explored a yield stress flow over a wide range of Bingham numbers, i.e., 0≤Bn≤1000. Flow aspects such as streamlines, yield boundaries, and unyielded zones were reported. It was stated that flow morphology at Bn=1000 and at Re in the range of 0.1-40 was identical. Most recently, M.B. Khan, et al. (2020) [22] carried out an intensive study of flow and heat transfer characteristics of a FENE-P-type viscoelastic fluid over a rotating cylinder. It was found that an inertio-elastic instability was induced at low rotational speeds that destabilized the flow; however, at high speeds, this instability gradually diminished and the flow became steady at Re=60 and 100. For the convection heat transfer, a correlation for the Nusselt number was proposed.

It is worth noting that the fluid in all of the aforementioned works is non-thixotropic. With a thixotropic material, as its microstructure and rheology can change under shearing conditions, its flow behaviours would become more complex than those of a simple yield-stress fluid. Indeed, in the flow of a thixotropic Bingham fluid past a stationary cylinder at Re=45 and Bn=0.5 and 5, reported by A. Syrakos, et al. (2015) [23], thixotropic parameters were found to significantly affect the flow field, especially the location and size of the unyielded or yielded zones.

In this work, we aim to further explore the flow behaviours of this type of fluid. In particular, we investigate the interaction of a thixotropic Bingham fluid with a rotating cylinder over a relatively wide range of Re, i.e., Re=20-100, and a dimensionless rotational speed of up to 5. Such a flow is expected to span from steady to unsteady laminar regimes. Special focus will be on a fluid layer surrounding the cylinder where the strain rate is large because of the rotation. Within this layer, the microstructure can be substantially broken resulting in an apparent viscosity as small as plastic viscosity, and thus the fluid can behave like a Newtonian one. This layer's effects on hydrodynamic forces will be examined.

Theory background

Governing equations

The mass and momentum equations for the fluid flow are, respectively, as follows:

$$\nabla \cdot \underline{u} = 0 \tag{1}$$

$$\frac{\partial(\rho \underline{u})}{\partial t} + \rho \underline{u} \cdot \nabla \underline{u} = \nabla \cdot \underline{\underline{\sigma}} \tag{2}$$

where $\underline{u}$ is the velocity, ρ the fluid density and $\underline{\underline{\sigma}} = -p\underline{\underline{I}} + \underline{\underline{\tau}}$ the total stress tensor. Moreover, p is the pressure, $\underline{\underline{I}}$ the unit tensor, and $\underline{\underline{\dot{\gamma}}}$ the deformation rate tensor defined as $\dot{\gamma}_{ij} = \frac{\partial u_i}{\partial x_j} + \frac{\partial u_j}{\partial x_i}$.

For a Newtonian fluid, $\underline{\underline{\tau}} = \mu \underline{\underline{\dot{\gamma}}}$, and for Bingham fluid, it is modeled as:

$$\begin{cases} \underline{\underline{\tau}} = \left(K + \dfrac{\tau_0}{\dot{\gamma}} \right) \underline{\underline{\dot{\gamma}}} & if\ \tau > \tau_0 \\ \dot{\gamma} = 0 & if\ \tau \le \tau_0 \end{cases} \tag{3}$$

Here, K is the consistency, $\dot{\gamma} = \sqrt{\frac{1}{2} \underline{\underline{\dot{\gamma}}} : \underline{\underline{\dot{\gamma}}}}$ is the strain rate tensor's magnitude, and $\tau = \sqrt{\frac{1}{2} \underline{\underline{\tau}} : \underline{\underline{\tau}}}$ is the intensity of the extra stress noting that $\dot{\gamma}$ and τ are scalars. As this model is discontinuous at $\tau=\tau_0$, regularization methods such as Papanastasiou's technique (1987) [24] and bi-viscosity approximations [25, 26] can be utilized to avoid singular possibilities. The former approach was proven to be more computationally reliable and efficient compared to bi-viscous ones [27]. It is hence employed in this work as:

$$\underline{\tau} = \left(K + \frac{\tau_0 [1 - exp(-m\dot{\gamma})]}{\dot{\gamma}} \right) \underline{\dot{\gamma}} \tag{4}$$

with m being the regularization parameter, which takes on a value of 40000 in this work. Note that when $m \to \infty$, Eq. (4) approaches Eq. (3) for an ideal HB fluid.

The Reynolds number is defined as $Re=\rho u_\infty D/K$ and the Bingham number as $Bn=\tau_y D/K u_\infty$ where D is the diameter of the cylinder, u_∞ the far field velocity, and τ_y the maximum yield stress. Furthermore, a dimensionless rotational speed α_r is defined as $\alpha_r=\omega D/2u_\infty$ with ω being the angular speed.

Thixotropy is modeled using a dimensionless structural parameter, λ, which takes on a value between 0 (completely unstructured) and 1 (fully structured). Specifically, its evolution follows a kinetic equation mimicking a reversible chemical reaction as [28]:

$$\frac{\partial \lambda}{\partial t} + \underline{u} \cdot \nabla \lambda = \alpha (1 - \lambda) - \beta \lambda \dot{\gamma} \tag{5}$$

where α and β are, respectively, the recovery and breakdown parameters. Accordingly, the first and the second terms on the right-hand side of Eq. (5) represent the recovery and the breakdown phenomena. The yield stress is determined as $\tau_0=\lambda\tau_y$ [29] with τ_y being the yield stress at $\lambda=1$. When $\lambda=0$, $\tau_0=0$, and the fluid becomes Newtonian.

Computational implementation

A two-dimensional (2D) computational domain employed in this work is shown in Fig. 1. It is a circular domain with a diameter $D_\infty=200D$. The inlet velocity

condition is applied to the front half of the domain's boundary while outlet pressure is applied to the rear half. In addition, a no-slip boundary condition is applied to the cylinder's surface. A structured mesh consisting of 92000 elements is generated in the domain. Results for strain rate profiles at several positions are shown in Fig. 2 and it is obvious that the mesh of 92000 elements is sufficient. Computation is carried out using ANSYS FLUENT augmented with User-Defined Functions (UDF) taking into account Eqs. (4) and (5). As Re is relatively low, i.e., 20≤Re≤100, the viscous-laminar model is employed.

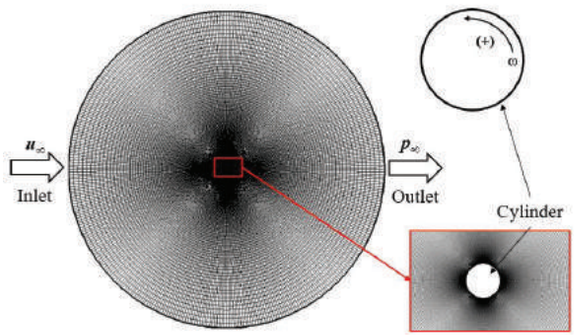

Fig. 1. Computational domain and mesh.

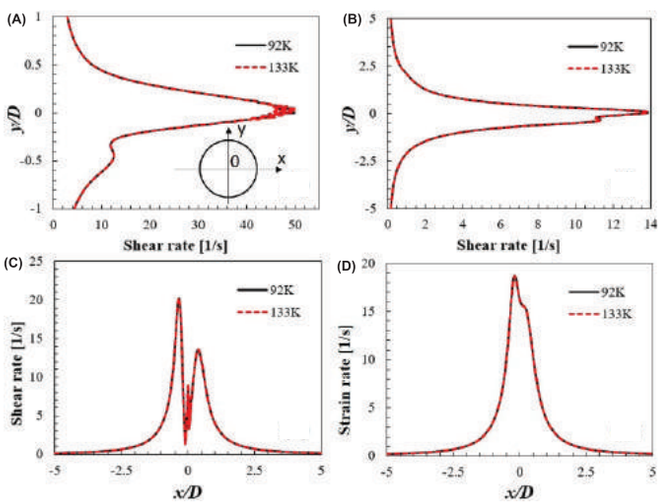

Fig. 2. Comparison of strain rate profiles along (A) *x*=0.501*D*, (B) x=0.51D, (C) y=-0.501D, and (D) y=-0.51D at Re=100, Bn=0.5, αr=5, α=0.05 and β=0.05 between a mesh of 92000 and a mesh of 133000 elements.

Results and discussion

Validation

For a stationary cylinder, results for the streamline pattern, the near-field unyielded zones, and the structural parameter of a thixotropic Bingham liquid at Re=45 and Bn=0.5 are shown in Fig. 3. Here, the breakdown parameter is β=0.05, and the recovery parameter takes on various values as α=0.01, 0.05, and 0.1. It is observed that under these conditions, the flow around the cylinder is in a steady laminar regime with a flow recirculation wake behind the cylinder. With a greater value of α, the fluid is more structured (large λ) especially inside the recirculation wake. The wake becomes smaller, whereas the unyielded zones become larger when α increases. These trends are well in line with those at the same conditions reported by A. Syrakos, et al. (2015) [23].

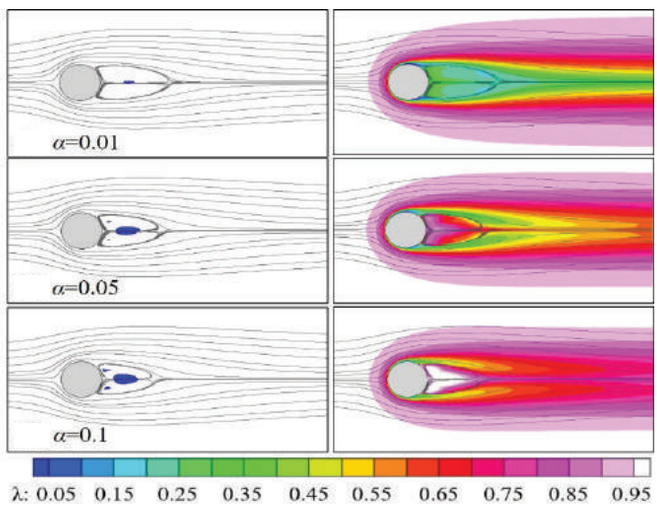

Fig. 3. Unyielded zones (left, dark areas) and distribution of *λ* (right) of a thixotropic flow at Re=45, Bn=0.5, β=0.05, and different values of *α*. Streamlines are shown on both sides; the cylinder is stationary.

For a rotating cylinder, results for drag (C_d) and lift (C_l) coefficients of a Newtonian fluid are compared with existing data. This is done for α_r=1 and Re=20, 40, and 100, and the results are presented in Table 1. It is noted that C_l can be positive or negative depending on the rotation direction; however, only its magnitude is shown. As can be seen, good agreement is achieved for all the cases. Furthermore, flow field morphology of a (non-thixotropic) Bingham liquid at α_r=0.5 and Re=0.1, 20, and 40 is presented in Fig. 4. Size and shape of the near-field unyielded and yielded zones are found to be in great agreement with those obtained by P. Thakur, et al. (2016) [21].

Table 1. C_d and C_l of a Newtonian fluid on a rotating cylinder at α_r=1.

	Present work		Reference data	
	Cd	*Cl*	*Cd*	*Cl*
Re=20	1.83	2.73	1.84 [20]; 1.84 [12]	2.75 [20]; 2.72 [12]
Re=40	1.32	2.59	1.32 [20]; 1.32 [12]	2.60 [20]; 2.60 [12]
Re=100	1.10	2.49	1.10 [12]; 1.11 [11]	2.50 [12]; 2.50 [11]

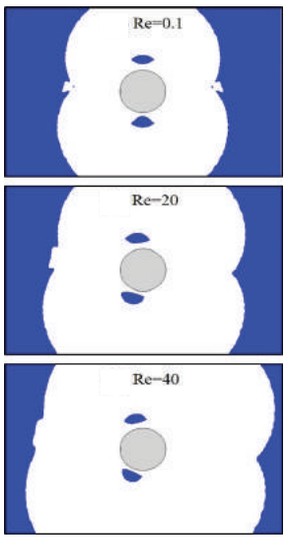

Fig. 4. Flow morphology of Bingham fluid at α_r=0.5, Bn=10, and Re=0.1, 20, and 40. Two unyielded zones are located above and below the cylinder.

Effect of the rotational speed

The effect of α_r on the flow field at Re=20, 45, and 100 is investigated in this section. To this end, various values of α_r ranging from 0 to 5 are realized. All the simulations are conducted at Bn=0.5, and with the thixotropic parameters of α=0.05 and β=0.05. Results for the streamlines and the near-field unyielded zones are shown in Fig. 5. It is obvious that when the cylinder is stationary (α_r=0), the flow is symmetrical at Re=20 and 45.

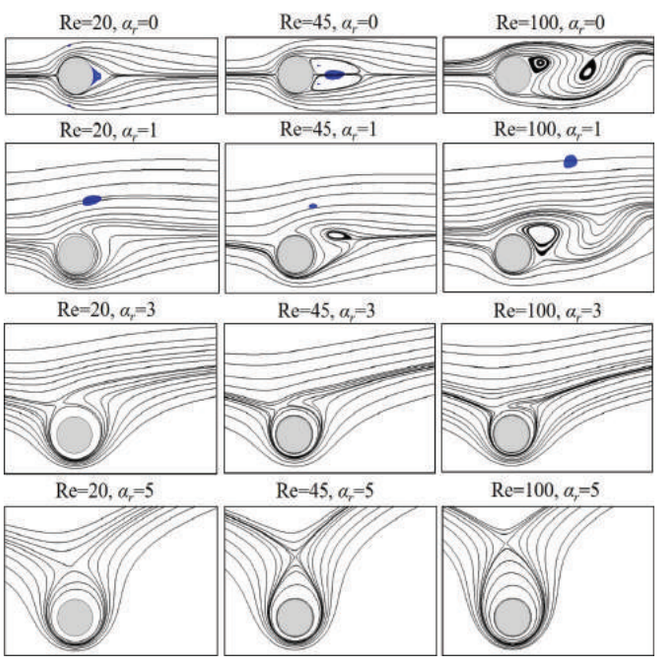

Fig. 5. Streamline pattern and unyielded zones (dark areas) at different rotational speeds (rows) and Re (columns).

A static, rigid zone is observed at Re=20, whereas three moving unyielded zones appear in the recirculation bubble behind the cylinder at Re=45. This finding is in line with A. Syrakos, et al. (2015) [23]. When the cylinder rotates ($\alpha_r \neq 0$), the symmetry no longer exists, and the rigid zones are pushed upward and away from the cylinder along the rotation direction. These zones are indeed not seen in proximity to the cylinder at α_r=3 and 5. At Re=100 (the highest Re investigated), the flow past the stationary cylinder is unsteady with periodic vortex shedding behind the cylinder. In addition, no rigid zones are observed near the cylinder at any rotational speeds.

Contours of the vorticity magnitude are shown in Fig. 6. As can be seen, the vortex shedding manifests only at Re=100 and α_r=0 and 1 although the vortex pattern is somewhat pushed upward at α_r=1. The flow becomes steady at greater rotational speeds, i.e., α_r=3 and 5.

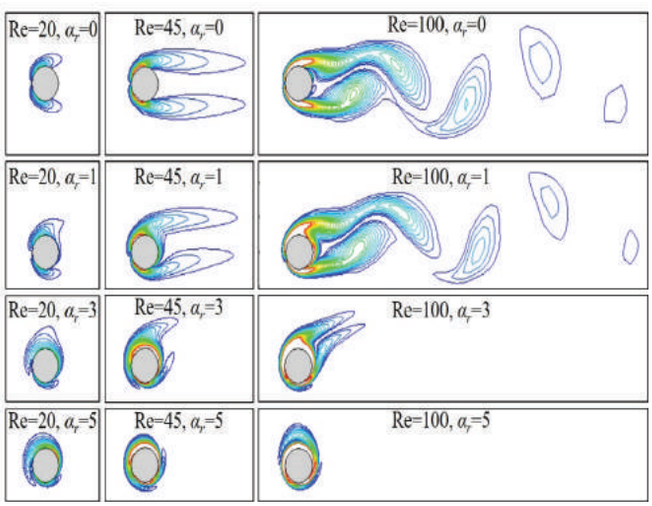

Fig. 6. Contours of the vorticity magnitude at different rotational speeds (rows) and Re (columns).

Results for the Strouhal number, St=fD/u_∞, where f is the vortex frequency, at α_r=0, 0.5, and 1 are provided in Table 2. It is noticed that St (thus f) of the non-thixotropic Bingham flow is smaller than that of the thixotropic Bingham and Newtonian flows at the same α_r. This trend of St can be attributed to the viscous effect, which is supposed to be greatest in non-thixotropic flows and smallest in Newtonian flows. In addition, St is found to slightly increase as α_r increases, especially for Bingham flows since their viscous effect becomes less important. It is worth mentioning that our results for the Newtonian flow at α_r=0 match perfectly with the experimental results of E. Berger and R. Wille (1972) [30] (St=0.16-0.17) and Williamson (1989) [31] (St=0.164).

Table 2. Strouhal number St at Re=100 and Bn=0.5.

Fluid	α_r=0	α_r=0.5	α_r=1
Newtonian	0.163	0.165	0.165
Thixotropic Bingham	0.160	0.165	0.165
Non-thixotropic Bingham	0.152	0.156	0.160

Furthermore, the distribution of the structural parameter λ at equilibrium is shown in Fig. 7 for Re=45 and α_r=5. The material is found to be substantially broken and becomes little structured ($\lambda \leq 0.05$) in a small region surrounding the cylinder. As the broken material passes the cylinder and moves to the downstream, its structure is gradually recovered and it reaches a fully structured state far behind the cylinder.

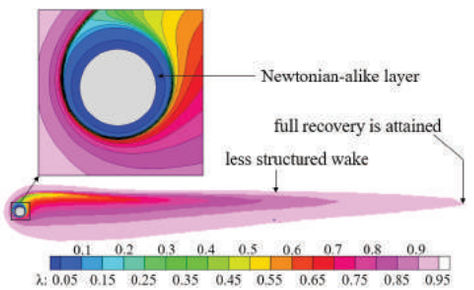

Fig. 7. Distribution of the structural parameter at Re=45, Bn=0.5, and α_r=5.

Additionally, the distribution of λ in close proximity to the cylinder is shown in Fig. 8 for various values of Re and α_r. It is noted that only $\lambda \leq 0.1$ is shown. A Newtonian-like layer is defined as $\lambda \leq 0.01$, which is equivalent to 99% of the microstructure having been broken, making the fluid essentially behave like a Newtonian one. This

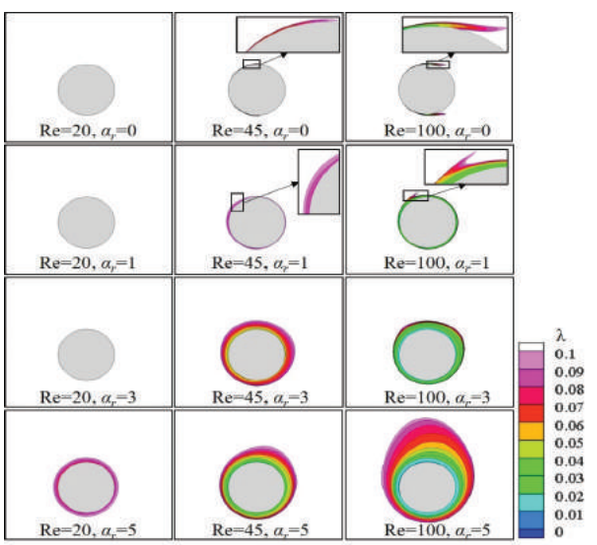

Fig. 8. Distribution of λ around the cylinder at different values of α_r (rows) and Re (columns).

layer turns out to be very thin and noticeable only at high values of Re (e.g., 45 and 100) and great rotational speeds (e.g., α_r=3 and 5).

The apparent viscosity of the Newtonian-like layer is expected to approach that of a Newtonian fluid, which is K according to Eq. (4). The results for the distribution of the apparent viscosity are presented in Fig. 9 in detail, which it is cut off at 1.1K.

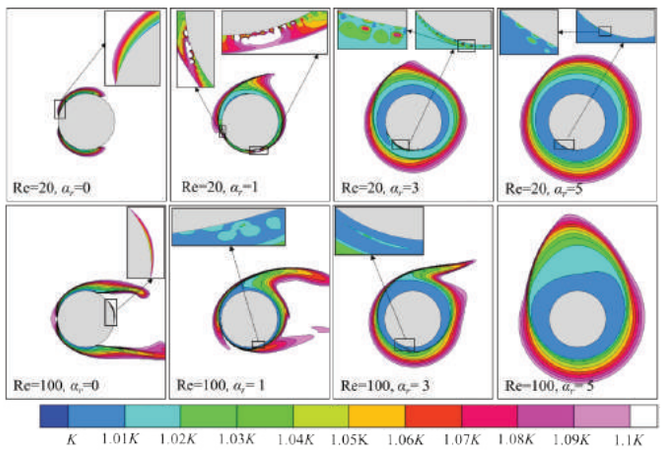

Fig. 9. Distribution of the apparent viscosity at Re=20 (top row) and Re=100 (bottom row) and different values of α_r.

It is obvious that the viscosity is not uniform, and in general it increases from the surface of the cylinder to the outside. For the stationary cylinder (α_r=0), the viscosity transition is quite smooth. However, for the rotating cylinder, the viscosity distribution is not continuous as small islands of greater viscosity appear within zones of small and constant viscosity. This phenomenon takes place below or on the lower part of the cylinder where two fluid motions meet and surpass each other. One fluid motion is caused by the rotation of the cylinder the other is the incoming flow. It is worth mentioning that the velocity of the former changes its direction as it flows along the surface. Fluid deformation is therefore expected to rapidly change from one point to another and can take on negative or positive values. As a consequence, the strain rate magnitude, defined as $\dot{\gamma} = \sqrt{\frac{1}{2}\dot{\underline{\underline{\gamma}}} : \dot{\underline{\underline{\gamma}}}}$, can be non-continuous as well as apparent viscosity. As Re and/or α_r increases, the viscosity distribution becomes more monotonous; indeed, at Re=100 and α_r=5, the mentioned viscosity islands are not found.

The non-continuous distribution of strain rate is observed also with Newtonian and non-thixotropic

Bingham fluids, as evident from Fig. 10 for Re=45 and α_r=5. In addition, it is noticed that the strain rate distribution of the three fluids in close proximity to the cylinder is almost identical, which can be attributed to the high rotational speed and thus high shear.

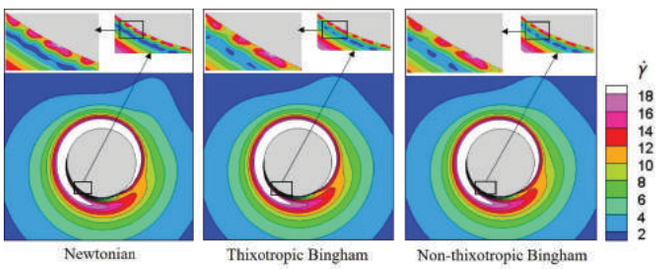

Fig. 10. Distribution of the strain rate for different fluids at Re=45 and α_r=5.

The Newtonian-like layer can be alternatively defined using the apparent viscosity, that is, $\mu_{app} \leq 1.01K$. This definition is pertinent to non-thixotropic fluids. Accordingly, as can be observed from Fig. 9, the thickness of this layer increases significantly as α_r increases, however, the effect of Re is less important. It is noteworthy that the two approaches (structure-wise and viscosity-wise) to defining the Newtonian-like layer result in a deviation of its thickness. Nevertheless, this follows the same trend as Re and/or α_r are varied (see Figs. 8 and 9).

Effect of the thixotropic parameters

Simulations for Re=45, Bn=0.5, α_r=1, and varying α and β (in the range from 0.001 to 1) are conducted. Here, focus is paid on the structural state λ in the region around the cylinder.

The distribution of λ at equilibrium is shown in Fig. 11 for different values of α, and that of the apparent viscosity is also shown therein. It is obvious that the material is more structured when α is greater, i.e., a greater structural recovery rate compared with the breakdown rate. Accordingly, the Newtonian-like layer defined by $\lambda \leq 0.01$ is thinner and becomes hardly observed for α=1. The same trend is observed when it is defined by $\mu_{app} \leq 1.01K$.

In a similar manner, the effect of β representing the breakdown rate is demonstrated in Fig. 12. As can be expected, it is opposite to the effect of α. The Newtonian-like layer can be clearly observed for β=1 but hardly noticed for β=0.001. Like the previous case and as mentioned earlier, the Newtonian-like layer is somewhat thicker and thus easier to be noticed when defined by $\mu_{app} \leq 1.01K$ than by $\lambda \leq 0.01$.

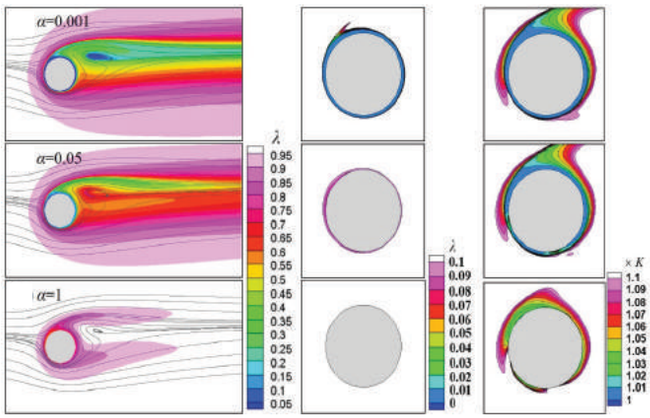

Fig. 11. Distributions of λ (left and middle) and apparent viscosity (right) for β=0.05 and various values of α; Re=45, Bn=0.5, and α_r=1.

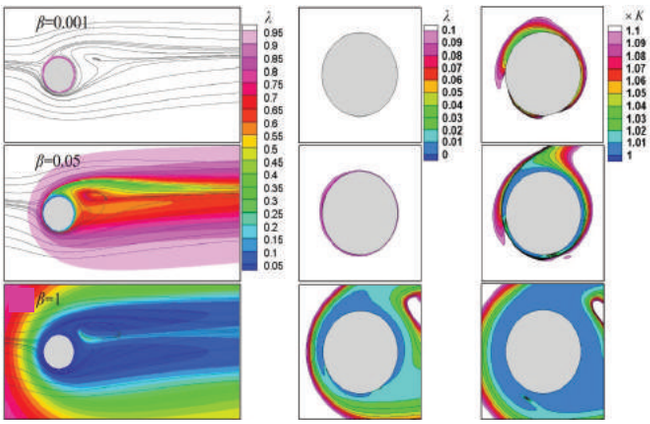

Fig. 12. Distributions of λ (left and middle) and apparent viscosity (right) for α=0.05 and various values of β; Re=45, Bn=0.5, and α_r=1.

Effect of Bn

The effect of the Bingham number on the thixotropic flow at Re=45 and 100 is examined here. To that end, simulations for Bn=1, 2, and 5 are performed. The other parameters are kept constant, that is, α=0.05, β=0.05, and α_r=1. Results for the streamline pattern and the unyielded zones are presented in Fig. 13. It is observed that no static rigid zones are formed under these conditions, similar to the case of Bn=0.5 presented in Fig. 5. Moving rigid zones are found to scatter in the flow field. They are closer to the cylinder at higher Bn. At Re=100, the flow regime is found to transition from a non-stationary laminar regime at Bn=1 to a stationary one at Bn=2 or higher. In addition, Fig. 14 shows the distribution of λ and the vorticity contours at Re=100 and Bn=1 and 2. It is noticed that the material is less structured in the wake of the cylinder, especially in areas of great vorticity. As Bn increases the wake (especially its less structured core resembling a tail) becomes narrower.

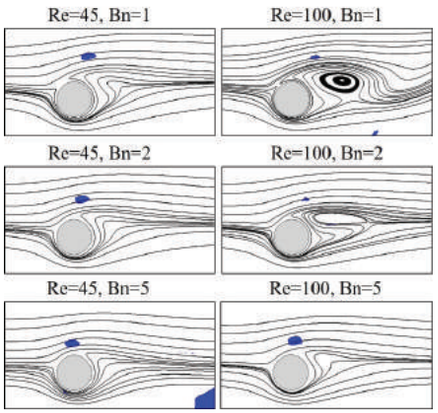

Fig. 13. Streamline pattern and unyielded zones (dark areas) of the thixotropic flow at Re=45 (left) and 100 (right), and different values of Bn; α_r=1.

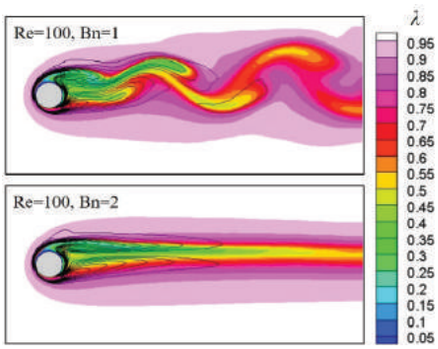

Fig. 14. Distribution of λ at Bn=1 and 2; Re=100 and α_r=1. Vorticity contours are also shown.

Furthermore, the distribution of the apparent viscosity is shown in Fig. 15. It is obvious that at a relatively low rotational speed, i.e., α_r=1, viscosity islands are found to exist and the Newtonian-like layer is not continuous, substantially thin, and becomes negligible as Bn increases to as high as 5.

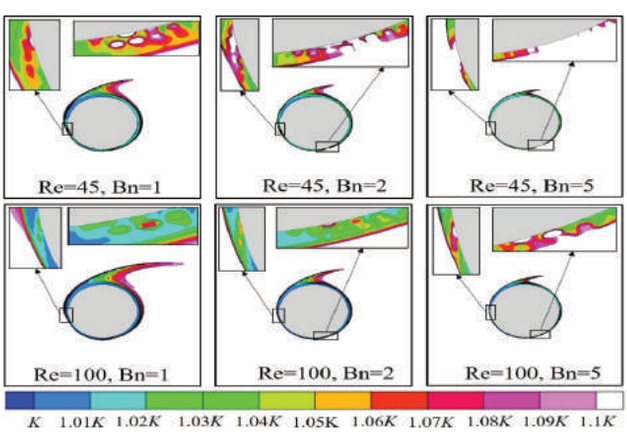

Fig. 15. Apparent viscosity at different values of Bn and Re=45 (top row) and 100 (bottom row).

Hydrodynamic forces

Results for C_d, C_l, and C_m are presented in Fig. 16 for various values of Re, Bn, and α_r. It is noted that $C \quad M/(0.5\ u_\infty AL)$ is the moment coefficient with M being the moment about z-axis, A the reference area, and L the length of the cylinder.

At the same Bn and rotational speed, the drag coefficient is found to be smaller at higher Re. At α_r=1, it increases approximately linearly with Bn with a slope being greater for Re=45 than for Re=100. In addition, it is noticed that the drag coefficient has a minimum value at α_r=3 for all Re conducted. S.K. Panda and R. Chhabra (2010) [20] also observed a similar trend for power-law liquids. However, more research may be needed for a better understanding of its governing mechanisms.

It is worth mentioning that as the rotation of the cylinder is counter-clockwise, C_l and C_m are always negative. Their magnitude (positive) is found to increase with increasing the rotational speed. The effect of Re on C_l is relatively small at $\alpha_r \leq 3$ and significant at higher α_r. Unlike C_d, C_l does not change its trend at this critical speed. The magnitude of C_m is seen to increase linearly with increasing α_r and Bn; this trend is more pronounced at smaller Re than at higher Re.

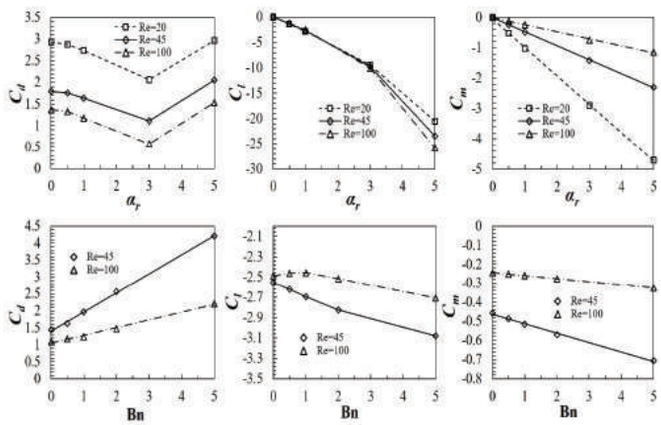

Fig. 16. C_d, C_l, and C_m versus α_r at Bn=0.5 (top row) and versus Bn at α_r=1 (bottom row).

A comparison of the hydrodynamic coefficients between Newtonian, thixotropic, and non-thixotropic Bingham fluids at Re=45 is presented in Fig. 17. It is noticed that C_d of the thixotropic fluid is somewhat smaller than that of the non-thixotropic fluid. They are both at Bn=0.5, however, as the microstructure of the former can be broken, its yield stress and thus apparent viscosity reduce especially in regions surrounding the cylinder and its wake. C_d of the equivalent Newtonian

fluid is considerably smaller. A negligible difference between C_l and C_m among the three fluids is observed. It is worth mentioning that the strain rate distribution of these fluids at α_r=5 in proximity to the cylinder is almost identical (see Fig. 10). The lift and moment coefficients can thus be postulated to be dictated by the fluid layer around the cylinder, which is typically the Newtonian-like layer.

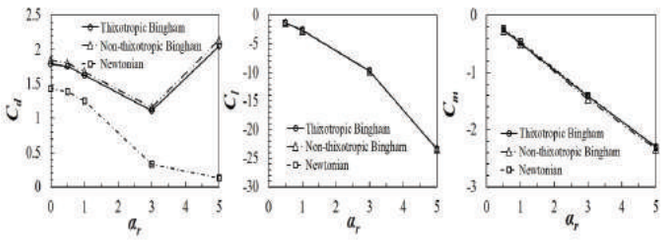

Fig. 17. Comparison of C_d, C_l, and C_m between three types of fluid at Re=45, Bn=0.5, and various values of α_r.

Furthermore, Fig. 18 shows the distribution of the static pressure coefficient, $C_p = 2(p - p_0)/(\rho u_\infty^2)$, on the cylinder's surface for various values of α_r. It is noticed that the pressure curve is symmetrical only for the case of stationary cylinder and at relatively low Re, i.e., Re=20 and 45. At Re=100, the flow becomes unsteady with periodic vortex shedding behind the cylinder and the C_p curve at any particular time instant is not necessarily symmetrical although it can be if averaged over a long enough time. For the case of a rotating cylinder ($\alpha_r \geq 0$), the symmetry is completely lost, and a minimum value of C_p is observed at ~270°. This minimum value decreases (negative) significantly with increasing rotational speed. Accordingly, the lift force (pointing downward) increases considerably as the rotational speed increases, which agrees with the C_l-α_r curve shown in Fig. 16.

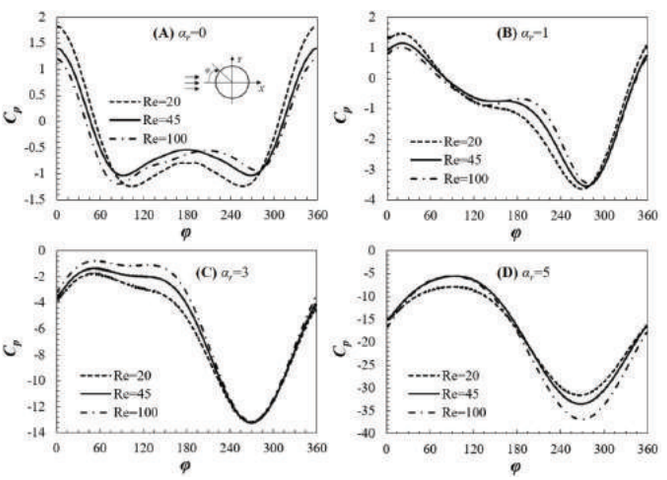

Fig. 18. Distribution of the static pressure on the cylinder's surface at various values of α_r; Bn=0.5.

Conclusions

The flow of a thixotropic Bingham fluid over a rotating cylinder has been studied using a numerical approach. The effects of the rotational speed, thixotropic parameters, Bn, and Re on the flow behaviours were investigated. Under the conditions realized, e.g., Re=20-100, Bn≤5, and $\alpha_r \leq 5$, the flow was laminar and steady except for the case of Re=100, Bn=0.5, and α_r=1 where it was unsteady with vortex shedding behind the cylinder.

The thixotropic material was less structured at higher rotational speeds. A region of low λ was observed around the cylinder, in which the yield stress and the apparent viscosity were small, and the fluid was believed to behave like a Newtonian one. Two definitions of the Newtonian-like layer were proposed, that is, $\lambda \leq 0.01$ and $\mu_{app} \leq 1.01K$. Its thickness was found to greatly depend on the rotational speed (i.e., greater at higher α_r) and, at relatively smaller extent, on the thixotropic parameters Re and Bn.

Results of C_d, C_l, and C_m were reported and discussed. They were found to significantly depend on the rotational speed, Re, and Bn. The magnitude of C_l and C_m increases with α_r and Bn, however, C_d was found to change its trend as it obtained a minimum value at α_r=3. More importantly, C_l and C_m of the Newtonian, thixotropic, and non-thixotropic Bingham fluids at Re=45 and Bn=0.5 were found to be close to one another and this was attributable to the Newtonian-like layer.

ACKNOWLEDGEMENTS

This research is funded by Vietnam National Foundation for Science and Technology Development (NAFOSTED) under grant number 107.03-2018.33.

COMPETING INTERESTS

The authors declare that there is no conflict of interest regarding the publication of this article.

REFERENCES

[1] M.I. Carretero, M. Pozo (2009), "Clay and non-clay minerals in the pharmaceutical industry: Part I. Excipients and medical applications", *Applied Clay Science*, **46(1)**, pp.73-80.

[2] J. Berlamont, M. Ockenden, E. Toorman, J. Winterwerp (1993), "The characterisation of cohesive sediment properties", *Coastal Engineering*, **21(1)**, pp.105-128.

[3] G. Chapman (1949), "The thixotropy and dilatancy of a marine soil", *Journal of the Marine Biological Association of the United Kingdom*, **28(1)**, pp.123-140.

[4] V. Osipov, S. Nikolaeva, V. Sokolov (1984), "Microstructural changes associated with thixotropic phenomena in clay soils", *Géotechnique*, **34(3)**, pp.293-303.

[5] R. Shaughnessy III, P.E. Clark (1988), "The rheological behavior of fresh cement pastes", *Cement Concrete Research*, **18(3)**, pp.327-341.

[6] B. Min, L. Erwin, H. Jennings (1994), "Rheological behaviour of fresh cement paste as measured by squeeze flow", *Journal of Materials Science*, **29(5)**, pp.1374-1381.

[7] J.E. Wallevik (2009), "Rheological properties of cement paste: Thixotropic behavior and structural breakdown", *Cement Concrete Research*, **39(1)**, pp.14-29.

[8] H.A. Barnes (1997), "Thixotropy - A review", *Journal of Non-Newtonian Fluid Mechanics*, **70(1-2)**, pp.1-33.

[9] J. Mewis, N. Wagner (2009), "Thixotropy", *Advances in Colloid Interface Science*, **147**, pp.214-227.

[10] R.G. Larson, Y. Wei (2019), "A review of thixotropy and its rheological modeling", *Journal of Rheology*, **63(3)**, pp.477-501.

[11] D. Stojković, M. Breuer, F. Durst (2002), "Effect of high rotation rates on the laminar flow around a circular cylinder", *Physics of Fluids*, **14(9)**, pp.3160-3178.

[12] S.B. Paramane, A. Sharma (2009), "Numerical investigation of heat and fluid flow across a rotating circular cylinder maintained at constant temperature in 2-D laminar flow regime", *International Journal of Heat Mass Transfer*, **52(13-14)**, pp.3205-3216.

[13] S. Karabelas (2010), "Large eddy simulation of high-Reynolds number flow past a rotating cylinder", *International Journal of Heat and Fluid Flow*, **31(4)**, pp.518-527.

[14] D.L. Tokpavi, A. Magnin, P. Jay (2008), "Very slow flow of Bingham viscoplastic fluid around a circular cylinder", *Journal of Non-Newtonian Fluid Mechanics*, **154(1)**, pp.65-76.

[15] S. Mossaz, P. Jay, A. Magnin (2010), "Criteria for the appearance of recirculating and non-stationary regimes behind a cylinder in a viscoplastic fluid", *Journal of Non-Newtonian Fluid Mechanics*, **165(21-22)**, pp.1525-1535.

[16] S. Mossaz, P. Jay, A. Magnin (2012a), "Non-recirculating and recirculating inertial flows of a viscoplastic fluid around a cylinder", *Journal of Non-Newtonian Fluid Mechanics*, **177-178**, pp.64-75.

[17] S. Mossaz, P. Jay, A. Magnin (2012b), "Experimental study of stationary inertial flows of a yield-stress fluid around a cylinder", *Journal of Non-Newtonian Fluid Mechanics*, **189-190**, pp.40-52.

[18] Z. Ouattara, P. Jay, D. Blésès, A. Magnin (2018), "Drag of a cylinder moving near a wall in a yield stress fluid", *AIChE Journal*, **64(11)**, pp.4118-4130.

[19] P. Townsend (1980), "A numerical simulation of Newtonian and visco-elastic flow past stationary and rotating cylinders", *Journal of Non-Newtonian Fluid Mechanics*, **6(3-4)**, pp.219-243.

[20] S.K. Panda, R. Chhabra (2010), "Laminar flow of power-law fluids past a rotating cylinder", *Journal of Non-Newtonian Fluid Mechanics*, **165(21-22)**, pp.1442-1461.

[21] P. Thakur, S. Mittal, N. Tiwari, R. Chhabra (2016), "The motion of a rotating circular cylinder in a stream of Bingham plastic fluid", *Journal of Non-Newtonian Fluid Mechanics*, **235**, pp.29-46.

[22] M.B. Khan, C. Sasmal, R. Chhabra (2020), "Flow and heat transfer characteristics of a rotating cylinder in a FENE-P type viscoelastic fluid", *Journal of Non-Newtonian Fluid Mechanics*, **282**, DOI: 10.1016/j.jnnfm.2020.104333.

[23] A. Syrakos, G.C. Georgiou, A.N. Alexandrou (2015), "Thixotropic flow past a cylinder", *Journal of Non-Newtonian Fluid Mechanics*, **220**, pp.44-56.

[24] T.C. Papanastasiou (1987), "Flows of materials with yield", *Journal of Rheology*, **31(5)**, pp.385-404.

[25] C. Beverly, R. Tanner (1989), "Numerical analysis of extrudate swell in viscoelastic materials with yield stress", *Journal of Rheology*, **33(6)**, pp.989-1009.

[26] S.S.P. Kumar, A. Vázquez-Quesada, M. Ellero (2020), "Numerical investigation of the rheological behavior of a dense particle suspension in a biviscous matrix using a lubrication dynamics method", *Journal of Non-Newtonian Fluid Mechanics*, **281**, DOI: 10.1016/j.jnnfm.2020.104312.

[27] Y. Fan, N. Phan-Thien, R.I. Tanner (2001), "Tangential flow and advective mixing of viscoplastic fluids between eccentric cylinders", *Journal of Fluid Mechanics*, **431**, pp.65-89.

[28] F. Moore (1959), "The rheology of ceramic slip and bodies", *J. Trans. Brit. Ceram. Soc.*, **58**, pp.470-492.

[29] E.A. Toorman (1997), "Modelling the thixotropic behaviour of dense cohesive sediment suspensions", *Rheologica Acta.*, **36(1)**, pp.56-65.

[30] E. Berger, R. Wille (1972), "Periodic flow phenomena", *Annual Review of Fluid Mechanics*, **4(1)**, pp.313-340.

[31] C. Williamson (1989), "Oblique and parallel modes of vortex shedding in the wake of a circular cylinder at low Reynolds numbers", *Journal of Fluid Mechanics*, **206**, pp.579-627.